Petroleum and Coal

Entropy-Generation Analysis of MHD Casson Nanofluid with Arrhenius Activation Energy and Chemical Reaction Effects

Adebowale Martins Obalalu

Department of Statistics and Mathematical Sciences, Kwara State University, Malete, Nigeria

Abstract

Current work studies the Impacts of binary chemical reaction, Arrhenius activation energy, second-order velocity slip, and solar radiation on Casson nanofluid induced by a stretching sheet. In the boundary layer region, nanoparticles provide an enhancement in the heat transfer phenomena. The equations obtained have been solved numerically using Galerkin weighted residual method (GWRM) and Gauss-Laguerre formula. he consistency and effectiveness of the Galerkin weighted residual method (GWRM) are confirmed by the residual errors. The obtained results were compared with those found in the literature to validate our method. Velocity, temperature, and nanoparticle volume fraction profiles are presented graphically and discussed. The results of the computation show that the effect of thermophysical properties such as Solar radiation parameter, suction/injection parameter, magnetic field parameter, and Eckert number on Skin friction coefficient (C_f) and local Nusselt number (N_u) more pronounced for Casson fluid when compare to the Newtonian fluid. The system stability at the molecular level reduces for Magnetic field parameter (M), however, significant amplification is described for Brinkman number, solar radiation parameter (N). understanding from the simulations are expected to help in managing the reservoir assets and making a consistent estimate about the production of oil and petroleum.

Keywords: *Solar radiation; Galerkin weighted residual method; Entropy generation; Arrhenius activation energy; and Chemical reaction.*

1. Introduction

Entropy generation is the quantity of disorderliness intensity when executing a basic conventional heat transfer. the second law has been utilized in different flow problems as well as the thermal system. The work of Bejan [1] is the fundamental study of entropy generation in fluid temperature. The study established the importance of temperature for entropy production through convectional heat transfer. Abolbashari *et al.* [2] presented a numerical investigation of entropy generation CF flow in a stretching surface. It was observed that the non-Newtonian Casson parameter boosts the entropy Generation number. Aziz *et al.* [3] studied a rectangular enclosure of CF with thermal radiation effect and chemical reaction. They reported that the entropy production intensifies while increasing the rheological parameter. Recently, Abd El-Aziz *at al.* [4] presented a second law analysis of MHD CF flow on a Stretching Sheet with a velocity slip. Their results revealed that the Casson parameter increases the heat transfer wall. Besides, Odesnya *et al.* [5] studied the possibility of entropy reduction generated in a viscous convection cooling system.

Solar radiation is one the best in sources of renewable energy with depressing environmental effect [6]. Solar radiation is the sum of energy which are released through the solar energy such as solar thermal energy. the study of radiative effect has become important due to the widespread in scientific and environmental processes such as heating, solar power technology, and electrical power generation where more details can be found in a review by [7]. Moreover, Turkyilmazoglu [8] studied the effect of thermal radiation on unsteady hydromagnetic permeable walls with variable viscosity. Their results revealed that the thermal radiation parameter

increased the temperature profile. Khan *et al.* [9] discusses the thermal radiation effect of viscous incompressible fluid flow with convective heating. Their results showed that the radiative parameter increases the temperature profile. Akhter *et al.* [10] discussed the effect of thermal radiation on Mhd natural convection boundary layer flow. Mondal *et al.* [11] considered the influence of thermal radiation on MHD asymmetric stagnant-point flow,

Casson fluid (CF) has received significant attention in numerous branches of many areas of science, engineering, and food processing [12]. Typical examples of common commodities exhibiting CF properties include oil, honey, jelly, and paints. CF model was first established by Casson [13]. The study establishes the prediction flow of pigment-oil suspension. Casson fluid is classified as a non-Newtonian fluid that exhibits shear thinning, yield stress, and high shear viscosity [15]. At low shear strain, it behaves like an elastic solid, while at above a critical yield stress it behaves like a Newtonian fluid [16]. Some common fluids that exhibit Casson fluid characteristics include jelly, blood, tomato paste, concentrated fruit juices, and shampoo [17]. [18] reported CF flow of hydromagnetic and thermal convection heat transfer in a stretched permeable surface. The authors affirmed that the enhancement in the non-Newtonian Casson parameter reduces the yield stress of the fluid flow and increases the fluid temperature. Shaw *et al*. [20] have studied Hydromagnetic Radiative CF flow through a vertical plate entrenched in a porous medium. Their results exhibited that the Casson parameter increases the fluid flow and decreases the temperature profile. Obalalu *et al.* [21] reported a numerical simulation of CF flow of Non-linear thermal convection with convective boundary conditions. The authors demonstrated that the velocity profile increases with the rheological parameter. Gireesha *et al.* [22] showed that the Newtonian fluid model reduced to non-Newtonian fluid especially when the wall stress is higher than the yield stress. Recently, Pop *et al.* [23] presented the thermal radiation effect on non-Newtonian CF in an enclosed space. The authors concluded that the rheological parameter enhances the fluid temperature. Gbadeyan *et al.* [24] employed a numerical method Galerkin method to investigate the hydromagnetic flow of a CF in the existence of a non-Darcian porous medium with variable thermal conductivity and viscosity effect. Their outcomes showed that the rheological parameter enhanced both the velocity and temperature profile.

Electrically conducting heat and mass carrier fluids which include water, mineral oil, ethylene glycol, etc. are important in research due to their applications in industry and engineering for industrial coolant, brake fluid, car radiator coolant, MHD generator, electronic voice coil cooling, nano-drug delivery, cancer therapy and so on [40-44]. However, these fluids have low thermophysical properties which obstruct their applications in the stated fields. Thermophysical properties of these fluids can be enhanced by adding ultrafine nanoparticles (usually made from metal or metallic oxide) into such fluids to have what is known as nanofluids. Nanofluids are found to possess higher thermal conductivity, boiling, and convective heat transfer performances compared to the conventional base fluid. Electrically conducting nanofluid can be manipulated using a magnetic field for diverse applications. These include wound treatment, gastric medication, sterilized devices, etc. [25]. Furthermore, magnetic nanoparticle-based bio-suspension have been reportedly used in magnetic resonance imaging (MRI), Hyperthermia, magnetic drug targeting (MDT), and tissue engineering (TE) [28].

Due to the various applications of nanofluids, researchers have been working on diverse ways to manufacture nanofluids. Jung *et al.* [27] investigated heat transfer and flow behaviors of TiO_2 nanofluid flowing upward in a vertical pipe. It was observed that the nanoparticle suspension enhanced fluid thermal conductivity. It was also found that the effective thermal conductivity of nanofluid for the smaller size of nanoparticles is larger than that of the bigger size at a given concentration. The heat transfer and laminar flow behaviors of Al_2O_3-water nanofluid in rectangular microchannels were experimentally studied by [28]. They discovered that the suspension of 1.8 percent nanoparticle concentration in nanofluid improved the heat transfer coefficient by 32 percent compared with water. Additional research works on nanofluid can also be found in [29-31].

Chemical reactions are highly important in chemical processing industries to transform cheap raw materials into high-value products. This can be achieved through a reactor that

brings reactants into close contact by providing suitable temperature and concentration fields for the duration of the process [32]. Boundary-layer flow involving binary mixture was first studied by Bestman [33]. The method used was the perturbation method and the effect of activation energy was examined.

In several fields of engineering, many researchers have solved various boundary element method (BEM) to establish the essential resolution to yield meaningful outcomes, such as the Homotopy Analysis Methods [17-19], Differential transformation method [20-22], Laplace transform [23], Galerkin weighted residual method (GWRM) [24-25], Lattice Boltzmann techniques [26], for symbolic programming codes, MATHEMATICA symbolic package [27], Maple Software [28], the algorithmic tools produce a reasonable framework for the fluid dynamitists with a magnificent multi-faceted method to predict a various array of nanofluid engineering problems.

Our review of the literature shows that while several methods including the weighted residual method been employed in the boundary layer of MHD Casson nanofluid flow, Arrhenius activation energy, and chemical reaction effects have not hitherto been investigated in the Galerkin weighted residual method (GWRM) and Gauss-Laguerre formula. thus, in this presented work, the distribution of the velocity fluid, heat transfer, Bejan number, and irreversibility rate over a shrinking, static, and stretching sheet was uplifted by the second law of thermodynamics. A model built on Galerkin weighted residual method was used to evaluate the heat and mass transfer in boundary layer Casson nanofluid flow with variable viscosity and thermal conductivity effect is presented, with the introduction of solar radiation term. motivated via the deficiency of investigation in this path "i.e." (the investigation that will yield correct outcomes and carryout well when the shear rate is not sufficiently low) despite its applications in science and technology.

2. Mathematical analysis

Consider a two-dimension incompressible Casson nanofluid of viscous electrically conducting extending directly over a stretching surface with the effect of Convective heating and velocity slip boundary conditions in a non-Darican porous medium as an exhibit in Fig 1. The fluid movement is laminar natural convective flow and steady. the contemporaneous result is conferred for velocity slips. it is assumed that the stretching sheet has a constant temperature and nanoparticle concentration T_∞ and C_∞ respectively, the magnetic fluid B_0 is fixed in a perpendicular path to the velocity flow.
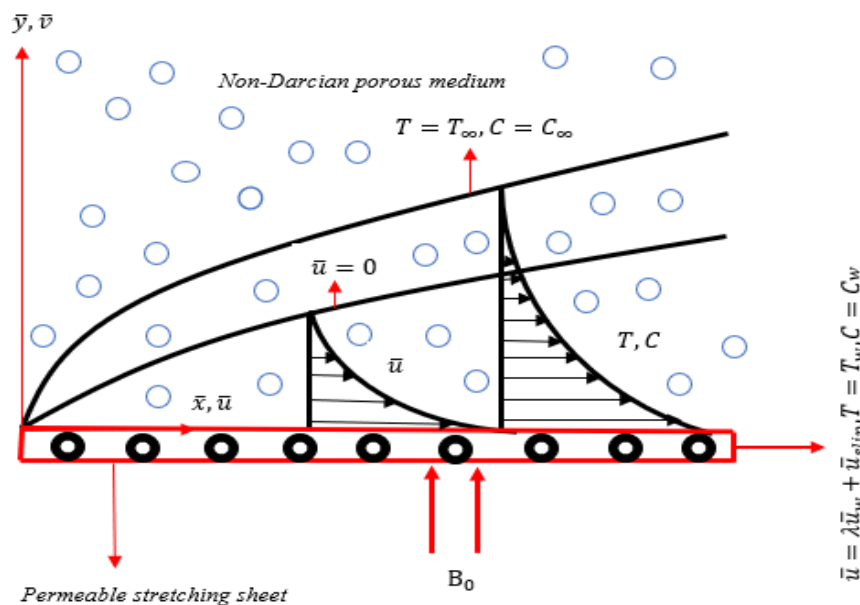

Figure 1a. Schematic depiction of the problem [21]

The rheological equation of an isotropic and incompressible flow of CF can be written as equation (1) [14].

$$\left.\begin{array}{l} \tau_{ij} = 2\left(\mu_B + \dfrac{P_y}{\sqrt{2\pi}}\right)e_{ij}\,\text{when}\,\pi > \pi_c \\[3mm] \tau_{ij} = 2\left(\mu_B + \dfrac{P_y}{\sqrt{2\pi c}}\right)e_{ij}\,\text{when}\,\pi < \pi_c \end{array}\right\} \tag{1}$$

P_y is the fluid yield stress of liquid and can expressed mathematically as

$$P_y = \frac{\mu_B\sqrt{2\pi}}{\beta} \tag{2}$$

Where

$$\mu_f = \mu_B + \frac{P_y}{\sqrt{2\pi}} \tag{3}$$

by substituting equation (2) into equation (3), the kinematic viscosity can be obtained as

$$\nu_f = \frac{\mu_B}{\rho_f}\left(1 + \frac{1}{\beta}\right) \tag{4}$$

β is the Casson parameter and the modified governing equations [21] are continuity Equation

$$\frac{\partial \bar{u}}{\partial \bar{x}} + \frac{\partial \bar{v}}{\partial \bar{y}} = 0 \tag{5}$$

Momentum equation

$$\bar{u}\frac{\partial \bar{u}}{\partial \bar{x}} + \bar{v}\frac{\partial \bar{v}}{\partial \bar{y}} = K\bar{U}_e\frac{d\bar{U}_e}{d\bar{x}} + \frac{\mu_B}{\rho_f}\left(1 + \frac{1}{\beta}\right)\frac{\partial^2 \bar{u}}{\partial \bar{y}^2} - \frac{\sigma_{0B^2(\bar{x})}}{\rho_f}(\bar{u}^2 - (K\bar{U}_e)^2) - \frac{b^*}{k_p}(\bar{u}^2 - (K\bar{U}_e)^2) \tag{6}$$
$$+ \frac{g}{\rho_f}\left[(1 - C_\infty)(T - T_\infty)\rho_{f\infty}\beta_0 - (\rho_p - \rho_{f\infty})(C - C_\infty)\right] - \frac{\mu_B}{\rho_f k_p}\left(1 + \frac{1}{\beta}\right)(\bar{u} - K\bar{U}_e)$$

Energy Equation

$$\bar{u}\frac{\partial T}{\partial \bar{x}} + \bar{v}\frac{\partial T}{\partial \bar{y}} = \alpha^*\frac{\partial^2 T}{\partial \bar{y}^2} + \tau\left[D_B\frac{\partial C}{\partial \bar{y}}\frac{\partial T}{\partial \bar{y}} + \frac{D_T}{T_\infty}\left(\frac{\partial T}{\partial \bar{y}}\right)^2\right] + \left(1 + \frac{1}{\beta}\right)\frac{\mu_B}{\rho_f c_p}\left(\frac{\partial \bar{u}}{\partial \bar{y}}\right)^2 - \frac{1}{\rho_f c_p}\frac{\partial q_r}{\partial \bar{y}} \tag{7}$$
$$+ \left(1 + \frac{1}{\beta}\right)\frac{\mu_B}{(\rho C_p)_f (k_p)_o}\bar{u}^2 + \frac{b^*}{(k_p)_o (C_p)_f}\bar{u}^3 + q''' + \frac{\sigma B_0^2}{(\rho C_p)_f}\bar{u}^2$$

Mass conversation

$$\bar{u}\frac{\partial C}{\partial \bar{x}} + \bar{v}\frac{\partial C}{\partial \bar{y}} = D_B\frac{\partial^2 C}{\partial \bar{y}^2} + \frac{D_T}{T_\infty}\frac{\partial^2 T}{\partial \bar{y}^2} - Kr(C - C_\infty)\left(\frac{T}{T_\infty}\right)^m e^{\frac{-E_a}{\kappa T}} \tag{8}$$

Entropy generation

$$N_G = \frac{K}{T_\infty^2}\left[1 + \frac{16\sigma_1 T_\infty^3}{3K}\right]\left[\left(\frac{\partial T}{\partial \bar{y}}\right)^2\right] + \frac{\mu}{T_\infty}\left(1 + \frac{1}{\beta}\right) + \left[\left(\frac{\partial \bar{u}}{\partial \bar{x}}\right)^2 + \left(\frac{\partial \bar{v}}{\partial \bar{y}}\right)^2\right] + \frac{\sigma_{0B_0^2}}{T_\infty}(v^2 + u^2) \tag{9}$$
$$+ \frac{RD}{C_\infty}\left[\left(\frac{\partial \bar{u}}{\partial \bar{x}}\right)^2 + \left(\frac{\partial \bar{v}}{\partial \bar{y}}\right)^2\right] + \frac{RD}{T_\infty}\left[\left(\frac{\partial \bar{u}}{\partial \bar{x}}\right)^2 + \left(\frac{\partial \bar{v}}{\partial \bar{y}}\right)^2\right] + \left[\left(\frac{\partial T}{\partial \bar{y}}\right)\left(\frac{\partial C}{\partial \bar{y}}\right)\right]$$

The corresponding boundary conditions are

$$\begin{cases} \bar{u} = \lambda\bar{u}_w(\bar{x}) + \bar{u}_{slip}, \bar{v} = v_w, T = T_w, C = C_w, \text{at}\,\bar{y} = 0 \\ \qquad\quad \bar{u} \to 0, T \to T_\infty, C \to C_\infty \text{ as } \bar{y} \to \infty \end{cases} \tag{10}$$

The term $\left(\frac{T}{T_\infty}\right)^m e^{\frac{-E_a}{\kappa T}}$ in eq. (8) denotes the modified Arrhenius function in which $\kappa = 8.61 \times 10^{-5}$ eV/K represents Boltzmann constant, m is the unitless exponent fitted rate constant $(-1 < m < 1)$ and E_a is the activation energy

The non-uniform heat source (or sink) q''' can be defined as [14]

$$q''' = \frac{k_\infty U_o}{2v_\infty\chi}[Q(T - T_\infty) + Q^*(T_W - T_\infty)\ell^{-\eta}] \tag{11}$$

Here heat generation is equivalent to $Q > 0, Q^* > 0$ also heat absorption is equivalent to $Q > 0, Q^* > 0$.

The Second-order velocity slip used is given as [46]

$$\overline{u}_{slip} = \frac{\mu_B}{\rho_f}\left(1+\frac{1}{\beta}\right)[(N_1)_o\frac{\partial\overline{u}}{\partial\overline{y}} + (N_2)_o\frac{\partial^2\overline{u}}{\partial\overline{y}^2}] \tag{12}$$

where $(N_2)_o < 0$ is the second-order velocity slip constant factor and $(N_1)_o > 0$ is the first order velocity slip constant factor. were introduced into $Eqs.(9) - (12)$ to obtain a set of ordinary nonlinear differential equations

$$u = \frac{\partial\psi}{\partial y} \; and \; v = -\frac{\partial\psi}{\partial x} \tag{13}$$

were introduced into $Eqs.(1) - (6)$ to obtain the following dimensionless equations

$$\frac{\partial\psi}{\partial y}\frac{\partial^2\psi}{\partial x\,\partial y} - \frac{\partial\psi}{\partial x}\frac{\partial^2\psi}{\partial y^2} = \left(1+\frac{1}{\beta}\right)\frac{\partial^3\psi}{\partial y^3} - M\frac{\partial\psi}{\partial y} - Pp\left(1+\frac{1}{\beta}\right)\frac{\partial\psi}{\partial y} - \frac{b^*L}{(k_p)_o}\left(\frac{\partial\psi}{\partial y}\right)^2 \tag{14}$$

$$\frac{\partial\psi}{\partial y}\frac{\partial\theta}{\partial x} - \frac{\partial\psi}{\partial x}\frac{\partial\theta}{\partial y} = \frac{1}{Pr}\frac{\partial^2\theta}{\partial y^2} + Nb\frac{\partial\theta}{\partial y}\frac{\partial\phi}{\partial y} + Nt\left(\frac{\partial\theta}{\partial y}\right)^2 + \frac{U_r^2}{(C_p)_f(T_w-T_\infty)}\left(1+\frac{1}{\beta}\right)\left(\frac{\partial^2\psi}{\partial y^2}\right)^2 + \frac{k_\infty U_o}{2\nu_\infty\chi}[Q(T-T_\infty)+ \tag{15}$$

$$Q^*(T_W-T_\infty)\ell^{-\eta}]\frac{b^*U_r^2L}{(C_p)_f(k_p)_o(T_w-T_\infty)}\left(\frac{\partial\psi}{\partial y}\right)^3 + \frac{\sigma B_0^2 U_r L}{\rho_f(C_p)_f(T_w-T_\infty)}\left(\frac{\partial\psi}{\partial y}\right)^2 + \frac{\nu U_r L}{(C_p)_f(k_p)_o(T_w-T_\infty)}\left(1+\frac{1}{\beta}\right)\left(\frac{\partial\psi}{\partial y}\right)^2.$$

$$Sc\frac{\partial\psi}{\partial y}\frac{\partial\phi}{\partial x} - Sc\frac{\partial\psi}{\partial x}\frac{\partial\phi}{\partial y} = \frac{\partial^2\phi}{\partial y^2} + \frac{Nt}{Nb}\frac{\partial^2\theta}{\partial y^2} - Sc\sigma^{*2}((Tr-1)\theta+1)^m e^{\frac{-E}{(Tr-1)\theta+1}} \tag{16}$$

$$\frac{Br}{\Omega}\left(1+\frac{1}{\beta}\right)\left(f'^2 + Ref''^2\right) + \frac{MPr}{\Omega}\left(f+Ref'^2\right) + \lambda\left(\frac{\epsilon}{\Omega}\right)\theta'(\eta) + \phi'(\eta) \tag{17}$$

with boundary conditions

$$\begin{cases} \frac{\partial\psi}{\partial y} = \lambda + \frac{\mu_B}{\rho_f}\left(1+\frac{1}{\beta}\right)\left(\frac{(N_1)_o\sqrt{Re}}{L}\frac{\partial^2\psi}{\partial y^2} + \frac{(N_2)_o Re}{L^2}\frac{\partial^3\psi}{\partial y^3}\right), \\ \frac{\partial\psi}{\partial x} = \frac{v_w\sqrt{Re}}{U_r}, \theta = 1, \phi = 1 \text{ at } y = 0 \\ \frac{\partial\psi}{\partial y} \to 0, \theta \to 0, \phi \to 0 \text{ as } y \to \infty \end{cases} \tag{18}$$

The following non-dimensional quantities were introduced:

$$\eta = y, \psi = xf(\eta), \theta = \theta(\eta), \phi = \phi(\eta), b^* = (b^*)_o x^{-1}, \tau = \frac{(\rho C_p)_p}{(\rho C_p)_f}, \alpha = \frac{k}{(\rho C_p)_f}, \nu = \frac{\mu_B}{\rho_f}\left(1+\frac{1}{\beta}\right), \overline{u}_w = \frac{U_r\overline{x}}{L}, x =$$

$$\frac{\overline{x}}{L}, y = \frac{\overline{y}\sqrt{Re}}{L}, u = \frac{\overline{u}}{U_r}, v = \frac{\overline{v}\sqrt{Re}}{U_r}, \theta = \frac{T-T_\infty}{T_w-T_\infty}, \phi = \frac{C-C_\infty}{C_w-C_\infty}, Pr = \frac{\nu}{\alpha}, Nb = \frac{\tau D_B(C_w-C_\infty)}{\nu}, Sc = \frac{\nu}{D_B}, \sigma^* = \frac{KrL}{U_r}, M =$$

$$\frac{\sigma B_0^2 L}{\rho_f U_r}, E = \frac{E_a}{\kappa T_\infty}, Pp = \frac{\nu L}{U_r(k_p)_o}, Ec = \frac{u_w}{(C_p)_f(T_w-T_\infty)}, Fs = \frac{(b^*)_o L}{(k_p)_o}, \delta_1 = \frac{(N_1)_o\mu_B\sqrt{Re}}{\rho_f L}(>0), \delta_2 =$$

$$\frac{(N_2)_o\mu_B Re}{\rho_f L^2}(<0), S = \frac{v_w\sqrt{Re}}{U_r}$$

$$\left(1+\frac{1}{\beta}\right)f''' + f''f - f'^2 - Mf' - Pp\left(1+\frac{1}{\beta}\right)f' - Fsf'^2 = 0 \tag{19}$$

$$\frac{1}{Pr}\theta'' + f\theta' + Nb\theta'\phi' + Nt\theta'^2 + Ec\left(1+\frac{1}{\beta}\right)f''^2 + EcMf'^2 + +EcPp\left(1+\frac{1}{\beta}\right)f'^2 \; EcFsf'^3 = 0 \tag{20}$$

$$\phi'' + \frac{Nt}{Nb}\theta'' + Scf\phi' - Sc\sigma^{*2}\phi((Tr-1)\theta+1)^m e^{\frac{-E}{(Tr-1)\theta+1}} = 0 \tag{21}$$

$$N_G = \frac{S''_{gen}}{s''} = Re(1+N)(\theta^2+\phi^2) + \frac{Br}{\Omega}\left(1+\frac{1}{\beta}\right)\left(f'^2+Ref''^2\right) + \frac{MPr}{\Omega}\left(f+Ref'^2\right) + \lambda\left(\frac{\epsilon}{\Omega}\right)\theta'(\eta) + \phi'(\eta) \tag{22}$$

with the corresponding boundary conditions

$$\begin{cases} f(0) = S, f'(0) = \lambda + \left(1+\frac{1}{\beta}\right)\left(\delta_1 f''(0) + \delta_2 f'''(0)\right), \theta(0) = 1, \phi(0) = 1 \\ f'(\infty) \to 0, \theta(\infty) \to 0, \phi(\infty) \to 0 \end{cases} \tag{23}$$

Other quantities of concern are the Bejan number, Nusselt number and Sherwood number which can be given as

$$S''_0 = \frac{R(DT)^2}{L^2 T_\infty^2}, Cf_{\overline{x}} = \frac{2\tau_w}{\rho U^2}, Nu_{\overline{x}} = \frac{-\overline{x}}{T_w - T_\infty}\left(\frac{\partial T}{\partial\overline{y}}\right)_{\overline{y}=0} \; and \; Sh_{\overline{x}} = \frac{-\overline{x}}{C_w - C_\infty}\left(\frac{\partial C}{\partial\overline{y}}\right)_{\overline{y}=0} \tag{24}$$

Using the similarity and dimensionless, we get

$$N_1 = Re(1+N)(\theta^2+\phi^2),$$

$$N_2 = \frac{Br}{\Omega}\left(1 + \frac{1}{\beta}\right)\left(f'^2 + Re f''^2\right) + \frac{MPr}{\Omega}\left(f + Re f'^2\right) + \lambda\left(\frac{\epsilon}{\Omega}\right)\theta'(\eta) + \phi'(\eta)$$

$$Nur = Re^{-\frac{1}{2}}Nu_{\overline{x}} = -\theta'(0) \ and \ Shr = Re^{-\frac{1}{2}}Sh_{\overline{x}} = -\phi'(0)$$

2.1. Application of weighted residual method

Applying the weighted residual method, we take the trial solutions for equ (18), (19) and (20),

$$f(\eta) = K\eta + \sum_{i=0}^{n} a_i e^{-\frac{i\eta}{4}}, \theta(\eta) = \sum_{i=1}^{n} b_i e^{-\frac{i\eta}{4}} and \phi(\eta) = \sum_{i=1}^{n} c_i e^{-\frac{i\eta}{4}} \tag{25}$$

$$f(0) = 0, \ f'(0) = \lambda + a\left(1 + \frac{1}{\beta}\right)f''(0), \ \theta(0) = 1 + b\theta'(0) \text{ and } \phi(0) = 1 + c\phi'(0) \tag{26}$$

chosen $n = 12$, then Put in equ (32) into the boundary conditions.

$$a_0 + a_1 + a_2 + a_3 + a_4 + a_5 + a_6 + a_7 + a_8 + a_9 + a_{10} + a_{11} + a_{12} = 0 \tag{27}$$

$$-\left(\frac{a_1}{16} + \frac{a_2}{4} + \frac{9a_3}{16} + a_4 + \frac{25a_5}{16} + \frac{9a_6}{4} + \frac{49a_7}{16} + 4a_8 + \frac{81a_9}{16} + \frac{25a_{10}}{4} + \frac{121a_{11}}{16} + 9a_{12}\right)a\left(\frac{1}{\beta} + 1\right) - a_4$$

$$- 2a_8 - 3a_{12} - \frac{a_2}{2} - \frac{3a_6}{2} - \frac{5a_{10}}{2} - \frac{a_1}{4} - \frac{3a_3}{4} - \frac{5a_5}{4} - \frac{7a_7}{4} - \frac{9a_9}{4} - \frac{11a_{11}}{4} - \lambda + K$$

$$= 0$$

$$-b\left(-\frac{b_1}{4} - b_4 - 2b_8 - 3b_{12} - \frac{b_2}{2} - \frac{3b_6}{2} - \frac{5b_{10}}{2} - \frac{3b_3}{4} - \frac{5b_5}{4} - \frac{7b_7}{4} - \frac{9b_9}{4} - \frac{11b_{11}}{4}\right) + b_1 + b_2 + b_3 + b_4 + \tag{28}$$
$$b_5 + b_6 + b_7 + b_8 + b_9 + b_{10} + b_{11} + b_{12} - 1 = 0$$

$$-c\left(-\frac{c_1}{4} - c_4 - 2c_8 - 3c_{12} - \frac{c_2}{2} - \frac{3c_6}{2} - \frac{5c_{10}}{2} - \frac{3c_3}{4} - \frac{5c_5}{4} - \frac{7c_7}{4} - \frac{9c_9}{4} - \frac{11c_{11}}{4}\right) \tag{29}$$

equ(21) satisfied automatically. Using equ (32) into equ (18), (19) and (20)lead to residuals

$$R_f = \frac{1}{Da}\left((1 + \frac{1}{\beta 1})\left(\frac{1}{4}e^{-\frac{\eta}{4}}a_1 + \frac{1}{2}e^{-\frac{\eta}{2}}a_2 + \frac{3}{4}e^{-\frac{3\eta}{4}}a_3 + e^{-\eta}a_4 + \frac{5}{4}e^{-\frac{5\eta}{4}}a_5 + \frac{3}{2}e^{-\frac{3\eta}{2}}a_6 + \frac{7}{4}e^{-\frac{7\eta}{4}}a_7\right.\right. \tag{30}$$

$$+ 2e^{-2\eta}a_8 + \frac{9}{4}e^{-\frac{9\eta}{4}}a_9 + \frac{5}{2}e^{-\frac{5\eta}{2}}a_{10} + \frac{11}{4}e^{-\frac{11\eta}{4}}a_{11} + 3e^{-3\eta}a_{12}) + (1$$

$$+ \frac{1}{\beta 1})\left(-\frac{1}{64}e^{-\frac{\eta}{4}}a_1 - \frac{1}{8}e^{-\frac{\eta}{2}}a_2 - \frac{27}{64}e^{-\frac{3\eta}{4}}a_3 - e^{-\eta}a_4 - \frac{125}{64}e^{-\frac{5\eta}{4}}a_5 - \frac{27}{8}e^{-\frac{3\eta}{2}}a_6\right.$$

$$- \frac{343}{64}e^{-\frac{7\eta}{4}}a_7 - 8e^{-2\eta}a_8 - \frac{729}{64}e^{-\frac{9\eta}{4}}a_9 - \frac{125}{8}e^{-\frac{5\eta}{2}}a_{10} - \frac{1331}{64}e^{-\frac{11\eta}{4}}a_{11}$$

$$- 27e^{-3\eta}a_{12}) + \frac{1}{4Pr}(2K - 2(K - \frac{1}{4}e^{-\frac{\eta}{4}}a_1 - \frac{1}{2}e^{-\frac{\eta}{2}}a_2 - \frac{3}{4}e^{-\frac{3\eta}{4}}a_3 - e^{-\eta}a_4$$

$$- \frac{5}{4}e^{-\frac{5\eta}{4}}a_5 - \frac{3}{2}e^{-\frac{3\eta}{2}}a_6$$

$$- \frac{7}{4}e^{-\frac{7\eta}{4}}a_7 - 2e^{-2\eta}a_8 - \frac{9}{4}e^{-\frac{9\eta}{4}}a_9 - \frac{5}{2}e^{-\frac{5\eta}{2}}a_{10} - \frac{11}{4}e^{-\frac{11\eta}{4}}a_{11} - 3e^{-3\eta}a_{12})^2 + 3(K\eta + a_0 + e^{-\frac{\eta}{4}}a_1$$

$$+ e^{-\frac{\eta}{2}}a_2 + e^{-\frac{3\eta}{4}}a_3 + e^{-\eta}a_4 + e^{-\frac{5\eta}{4}}a_5 + e^{-\frac{3\eta}{2}}a_6 + e^{-\frac{7\eta}{4}}a_7 + e^{-2\eta}a_8 + e^{-\frac{9\eta}{4}}a_9$$

$$+ e^{-\frac{5\eta}{2}}a_{10} + e^{-\frac{11\eta}{4}}a_{11} + e^{-3\eta}a_{12})(\frac{1}{16}e^{-\frac{\eta}{4}}a_1 + \frac{1}{4}e^{-\frac{\eta}{2}}a_2 + \frac{9}{16}e^{-\frac{3\eta}{4}}a_3 + e^{-\eta}a_4$$

$$+ \frac{25}{16}e^{-\frac{5\eta}{4}}a_5 + \frac{9}{4}e^{-\frac{3\eta}{2}}a_6 + \frac{49}{16}e^{-\frac{7\eta}{4}}a_7 + 4e^{-2\eta}a_8 + \frac{81}{16}e^{-\frac{9\eta}{4}}a_9 + \frac{25}{4}e^{-\frac{5\eta}{2}}a_{10}$$

$$+ \frac{121}{16}e^{-\frac{11\eta}{4}}a_{11} + 9e^{-3\eta}a_{12} + 4M(K^2 - (K - \frac{1}{4}e^{-\frac{\eta}{4}}a_1 - \frac{1}{2}e^{-\frac{\eta}{2}}a_2 - \frac{3}{4}e^{-\frac{3\eta}{4}}a_3$$

$$- e^{-\eta}a_4 - \frac{5}{4}e^{-\frac{5\eta}{4}}a_5 - \frac{3}{2}e^{-\frac{3\eta}{2}}a_6 - \frac{7}{4}e^{-\frac{7\eta}{4}}a_7 - 2e^{-2\eta}a_8 - \frac{9}{4}e^{-\frac{9\eta}{4}}a_9 - \frac{5}{2}e^{-\frac{5\eta}{2}}a_{10}$$

$$- \frac{11}{4}e^{-\frac{11\eta}{4}}a_{11} - 3e^{-3\eta}a_{12})^2) + 4\alpha(K^2 - (K - \frac{1}{4}e^{-\frac{\eta}{4}}a_1 - \frac{1}{2}e^{-\frac{\eta}{2}}a_2 - \frac{3}{4}e^{-\frac{3\eta}{4}}a_3$$

$$- e^{-\eta}a_4 - \frac{5}{4}e^{-\frac{5\eta}{4}}a_5 - \frac{3}{2}e^{-\frac{3\eta}{2}}a_6 - \frac{7}{4}e^{-\frac{7\eta}{4}}a_7 - 2e^{-2\eta}a_8 - \frac{9}{4}e^{-\frac{9\eta}{4}}a_9 - \frac{5}{2}e^{-\frac{5\eta}{2}}a_{10}$$

$$- \frac{11}{4}e^{-\frac{11\eta}{4}}a_{11} - 3e^{-3\eta}a_{12})^2)) + e^{-\frac{\eta}{4}}b_1 + e^{-\frac{\eta}{2}}b_2 + e^{-\frac{3\eta}{4}}b_3 + e^{-\eta}b_4 + e^{-\frac{5\eta}{4}}b_5$$

$$+ e^{-\frac{3\eta}{2}}b_6 + e^{-\frac{7\eta}{4}}b_7 + e^{-2\eta}b_8 + e^{-\frac{9\eta}{4}}b_9 + e^{-\frac{5\eta}{2}}b_{10} + e^{-\frac{11\eta}{4}}b_{11} + e^{-3\eta}b_{12} - Nr(e^{-\frac{\eta}{4}}c_1$$

$$+ e^{-\frac{\eta}{2}}c_2 + e^{-\frac{3\eta}{4}} + e^{-\eta}c_4 + e^{-\frac{5\eta}{4}}c_5 + e^{-\frac{3\eta}{2}}c_6 + e^{-\frac{7\eta}{4}}c_7 + e^{-2\eta}c_8 + e^{-\frac{9\eta}{4}}c_9 + e^{-\frac{5\eta}{2}}c_{10}$$

$$+ e^{-\frac{11\eta}{4}}c_{11} + e^{-3\eta}c_{12}),$$

$$R_\theta = \text{EcPr}(1 + \frac{1}{\beta 1})(\frac{1}{16}e^{-\frac{\eta}{4}}a_1 + \frac{1}{4}e^{-\frac{\eta}{2}}a_2 + \frac{9}{16}e^{-\frac{3\eta}{4}}a_3 + e^{-\eta}a_4 + \frac{25}{16}e^{-\frac{5\eta}{4}}a_5 \; e^{-\frac{3\eta}{2}}a_6 + \frac{49}{16}e^{-\frac{7\eta}{4}}a_7 + \tag{31}$$

$$4e^{-2\eta}a_8 + \frac{81}{16}e^{-\frac{9\eta}{4}}a_9 + \frac{25}{4}e^{-\frac{5\eta}{2}}a_{10} + \frac{121}{16}e^{-\frac{11\eta}{4}}a_{11} \; 9e^{-3\eta}a_{12})^2 + \text{Nt}(-\frac{1}{4}e^{-\frac{\eta}{4}}b_1 - \frac{1}{2}e^{-\frac{\eta}{2}}b_2 - \frac{3}{4}e^{-\frac{3\eta}{4}}b_3 -$$

$$e^{-\eta}b_4 - \frac{5}{4}e^{-\frac{5\eta}{4}}b_5 - \frac{3}{2}e^{-\frac{3\eta}{2}}b_6 - \frac{7}{4}e^{-\frac{7\eta}{4}}b_7 - 2e^{-2\eta}b_8 - \frac{9}{4}e^{-\frac{9\eta}{4}}b_9 - \frac{5}{2}e^{-\frac{5\eta}{2}}b_{10} - \frac{11}{4}e^{-\frac{11\eta}{4}}b_{11} -$$

$$3e^{-3\eta}b_{12})^2 + \frac{1}{16}e^{-\frac{\eta}{4}}b_1 + \frac{1}{4}e^{-\frac{\eta}{2}}b_2 + \frac{9}{16}e^{-\frac{3\eta}{4}}b_3 + e^{-\eta}b_4 + \frac{25}{16}e^{-\frac{5\eta}{4}}b_5 + \frac{9}{4}e^{-\frac{3\eta}{2}}b_6 + \frac{49}{16}e^{-\frac{7\eta}{4}}b_7 + 4e^{-2\eta}b_8 +$$

$$\frac{81}{16}e^{-\frac{9\eta}{4}}b_9 + \frac{25}{4}e^{-\frac{5\eta}{2}}b_{10} + \frac{121}{16}e^{-\frac{11\eta}{4}}b_{11} + 9e^{-3\eta}b_{12} + \frac{3}{4}(K\eta + a_0 + e^{-\frac{\eta}{4}}a_1 + e^{-\frac{\eta}{2}}a_2 + e^{-\frac{3\eta}{4}}a_3 + e^{-\eta}a_4 +$$

$$e^{-\frac{5\eta}{4}}a_5 + e^{-\frac{3\eta}{2}}a_6 + e^{-\frac{7\eta}{4}}a_7 + e^{-2\eta}a_8 + e^{-\frac{9\eta}{4}}a_9 + e^{-\frac{5\eta}{2}}a_{10} + e^{-\frac{11\eta}{4}}a_{11} + e^{-3\eta}a_{12})(-\frac{1}{4}e^{-\frac{\eta}{4}}b_1 -$$

$$\frac{1}{2}e^{-\frac{\eta}{2}}b_2 - \frac{3}{4}e^{-\frac{3\eta}{4}}b_3 - e^{-\eta}b_4 - \frac{5}{4}e^{-\frac{5\eta}{4}}b_5 - \frac{3}{2}e^{-\frac{3\eta}{2}}b_6 - \frac{7}{4}e^{-\frac{7\eta}{4}}b_7 - 2e^{-2\eta}b_8 - \frac{9}{4}e^{-\frac{9\eta}{4}}b_9 - \frac{5}{2}e^{-\frac{5\eta}{2}}b_{10} -$$

$$\frac{11}{4}e^{-\frac{11\eta}{4}}b_{11} - 3e^{-3\eta}b_{12} + \frac{4}{3\text{Ra1}}((\frac{1}{16}e^{-\frac{\eta}{4}}b_1 + \frac{1}{4}e^{-\frac{\eta}{2}}b_2 + \frac{9}{16}e^{-\frac{3\eta}{4}}b_3 + e^{-\eta}b_4 + \frac{25}{16}e^{-\frac{5\eta}{4}}b_5 + \frac{9}{4}e^{-\frac{3\eta}{2}}b_6 +$$

$$\frac{49}{16}e^{-\frac{7\eta}{4}}b_7 + 4e^{-2\eta}b_8 + \frac{81}{16}e^{-\frac{9\eta}{4}}b_9 + \frac{25}{4}e^{-\frac{5\eta}{2}}b_{10} + \frac{121}{16}e^{-\frac{11\eta}{4}}b_{11} + ((\text{tr} - 1)(e^{-\frac{\eta}{4}}b_1 + e^{-\frac{\eta}{2}}b_2 + e^{-\frac{3\eta}{4}}b_3 +$$

$$e^{-\eta}b_4 + e^{-\frac{5\eta}{4}}b_5 + e^{-\frac{3\eta}{2}}b_6 + e^{-\frac{7\eta}{4}}b_7 + e^{-2\eta}b_8 + b_9e^{-\frac{5\eta}{2}}b_{10} + e^{-\frac{11\eta}{4}}b_{11} + e^{-3\eta}b_{12}) + 1)^3 + 3(\text{tr} -$$

$$1)(-\frac{1}{4}e^{-\frac{\eta}{4}}b_1 - \frac{1}{2}e^{-\frac{\eta}{2}}b_2 - \frac{3}{4}e^{-\frac{3\eta}{4}}b_3e^{-\eta}b_4 - \frac{5}{4}e^{-\frac{5\eta}{4}}b_5 - \frac{3}{2}e^{-\frac{3\eta}{2}}b_6 - \frac{7}{4}e^{-\frac{7\eta}{4}}b_7 - 2e^{-2\eta}b_8 - \frac{9}{4}e^{-\frac{9\eta}{4}}b_9 -$$

$$\frac{5}{2}e^{-\frac{5\eta}{2}}b_{10}\frac{11}{4}e^{-\frac{11\eta}{4}}b_{11} - 3e^{-3\eta}b_{12})^2((\text{tr} - 1)(e^{-\frac{\eta}{4}}b_1 + e^{-\frac{\eta}{2}}b_2 + e^{-\frac{3\eta}{4}}b_3 + e^{-\eta}b_4 + e^{-\frac{5\eta}{4}}b_5 + e^{-\frac{7\eta}{4}}b_7 +$$

$$e^{-2\eta}b_8 + e^{-\frac{9\eta}{4}}b_9 + e^{-\frac{5\eta}{2}}b_{10} + e^{-\frac{11\eta}{4}}b_{11} + e^{-3\eta}b_{12}) + 1)^2) + \text{Nb}(-\frac{1}{4}e^{-\frac{\eta}{2}}b_2 - \frac{3}{4}e^{-\frac{3\eta}{4}}b_3 - e^{-\eta}b_4 -$$

$$\frac{5}{4}e^{-\frac{5\eta}{4}}b_5 - \frac{3}{2}e^{-\frac{3\eta}{2}}b_6 - \frac{7}{4}e^{-\frac{7\eta}{4}}b_7 - 2e^{-2\eta}b_8 - \frac{9}{4}\frac{5}{2}e^{-\frac{5\eta}{2}}b_{10} - \frac{11}{4}e^{-\frac{11\eta}{4}}b_{11} -$$

$$R_\phi = \frac{3}{4}\text{Le}(-\frac{1}{4}c_1e^{-\frac{\eta}{4}} - \frac{1}{2}c_2e^{-\frac{\eta}{2}} - \frac{3}{4}c_3e^{-\frac{3\eta}{4}} - c_4e^{-\eta} - \frac{5}{4}c_5e^{-\frac{5\eta}{4}} - \frac{3}{2}c_6e^{-\frac{3\eta}{2}} - \frac{7}{4}c_7e^{-\frac{7\eta}{4}} \tag{32}$$

$$- 2c_8e^{-2\eta} - \frac{9}{4}c_9e^{-\frac{9\eta}{4}} - \frac{5}{2}c_{10}e^{-\frac{5\eta}{2}} - \frac{11}{4}c_{11}e^{-\frac{11\eta}{4}} - 3c_{12}e^{-3\eta})(a_1e^{-\frac{\eta}{4}}$$

$$+ a_2e^{-\frac{\eta}{2}} + a_3e^{-\frac{3\eta}{4}} + a_4e^{-\eta} + a_5e^{-\frac{5\eta}{4}} + a_6e^{-\frac{3\eta}{2}} + a_7e^{-\frac{7\eta}{4}} + a_8e^{-2\eta}$$

$$+ a_9e^{-\frac{9\eta}{4}} + a_{10}e^{-\frac{5\eta}{2}} + a_{11}e^{-\frac{11\eta}{4}} + a_{12}e^{-3\eta} + a_0 + \eta K) + \frac{\text{Nt}}{\text{Nb}}(\frac{1}{16}b_1e^{-\frac{\eta}{4}}$$

$$+ \frac{1}{4}b_2e^{-\frac{\eta}{2}} + \frac{9}{16}b_3e^{-\frac{3\eta}{4}} + b_4e^{-\eta} + \frac{25}{16}b_5e^{-\frac{5\eta}{4}} + \frac{9}{4}b_6e^{-\frac{3\eta}{2}} + \frac{49}{16}b_7e^{-\frac{7\eta}{4}}$$

$$+ 4b_8e^{-2\eta} + \frac{81}{16}b_9e^{-\frac{9\eta}{4}} + \frac{25}{4}b_{10}e^{-\frac{5\eta}{2}} + \frac{121}{16}b_{11}e^{-\frac{11\eta}{4}} + 9b_{12}e^{-3\eta})$$

$$+ \frac{1}{16}c_1e^{-\frac{\eta}{4}} + \frac{1}{4}c_2e^{-\frac{\eta}{2}} + \frac{9}{16}c_3e^{-\frac{3\eta}{4}} + c_4e^{-\eta} + \frac{25}{16}c_5e^{-\frac{5\eta}{4}} + \frac{9}{4}c_6e^{-\frac{3\eta}{2}}$$

$$+ \frac{49}{16}c_7e^{-\frac{7\eta}{4}} + 4c_8e^{-2\eta} + \frac{81}{16}c_9e^{-\frac{9\eta}{4}} + \frac{25}{4}c_{10}e^{-\frac{5\eta}{2}} + \frac{121}{16}c_{11}e^{-\frac{11\eta}{4}}$$

$$+ 9c_{12}e^{-3\eta}.$$

Utilize the Galerkin method via putting the integral of the result of residuals and the weighting functions $e^{-\frac{i\eta}{4}}$, for $i = 0,1,2,\dots,10$ to zero, we have

$$\int_0^\infty R_f e^{-\frac{i\eta}{4}}d\eta = 0, \int_0^\infty R_\theta e^{-\frac{i\eta}{4}}d\eta = 0 \text{ and } \int_0^\infty R_\phi e^{-\frac{i\eta}{4}}d\eta = 0, \tag{33}$$

We have **37** nonlinear equations through equations $(34) - (36)$. Setting the following values of parameters $\text{Ec} = 0.01, \text{Le} = 5, \text{Nr} = 1, \text{Nb} = 0.1, \text{Nt} = 0.1, \text{ Pr} = 6.8, \; a = 0.1, \; b = 0.1, \; c = 0.1, \; K = 1, \; \text{Da} = 10, \; \alpha = 0.1, \; N = 15, \; \text{Tr} = 2, \; \beta = 0.5, \; M = 0.5 \text{ and } \lambda = -0.5$
we obtain the values of constants $a_i, \; b_i$ and c_i through the assist of MATHEMATICA symbolic package.

$$a_0 = -2.12187, a_1 = -0.0163122, a_2 = 0.490342, a_3 = 6.03219, a_4 = -17.987, \tag{34}$$
$$a_5 = 50.0422, a_6 = -168.838, a_7 = 445.916, a_8 = -714.239, a_9 = 677.765,$$
$$a_{10} = -374.375, a_{11} = 110.713, a_{12} = -13.3812, b_1 = -0.0123395, b_2 = 1.38074,$$
$$b_3 = -41.8527, b_4 = 554.722, b_5 = -3873.5, b_6 = 15612.8, b_7 = -38284.9,$$
$$b_8 = 59291.5, b_9 = -58557.1, b_{10} = 35886.8, b_{11} = -12471.7, b_{12} = 1882.47,$$
$$c_1 = -0.0134059, c_2 = 1.43805, c_3 = -44.0556, c_4 = 611.46, c_5 = -4609.9,$$
$$c_6 = 20693.8, c_7 = -58122.4, c_8 = 104560., c_9 = -120206., c_{10} = 85331.1,$$
$$c_{11} = -34062.7, c_{12} = 5849.05$$

2.2. The Gauss-Laguerre formula

Now we apply Gauss-Laguerre formula, Subsequently the sphere ranges from $0 \leq \xi \leq \infty$) [21]:

$$\int_0^\infty e^{-x} f(x) dx = \sum_{k=1}^n A_k f(x_k) + \frac{(n!)^2}{(2n)!} f^{(2n)}(\xi). \tag{35}$$

Given that

$$\int_0^\infty e^{-x} f(x) dx \approx \sum_{k=1}^n A_k f(x_k), \tag{36}$$

We obtain the the coefficients A_k as [21]

$$A_k = \frac{1}{L'_n(x_k)} \int_0^\infty \frac{L_n(x) e^{-x}}{x - x_k} dx = \frac{(n!)^2}{x_k (L'_n(x_k))^2}, \tag{37}$$

Then x_k remain the zeroes of the nth Laguerre pollynomial

$$L_n = e^x \frac{d^n}{dx^n} (e^{-x} x^n) \tag{38}$$

Taken $n = 10$, for instance, Table 1 displays the values of x_k and coefficients values of A_k. Finally, MATHEMATICAL software was used to compute the unknown coefficients.

Table 1. Arguments x_k and coefficients A_k

x_k	A_k
0.137793470540492	0.308441115765020
0.729454549503171	0.401119929155277
1.808342901740317	0.218068287611810
3.401433697854960	0.062087456098682
5.552496140063418	0.009501516975185
8.330152746764144	0.000753008388591
11.843785837899944	0.000028259233496
16.279257831377613	$4.249313985004240 \times 10^{-7}$
21.996585811980830	$1.839564823966167 \times 10^{-9}$
29.920697012273720	$9.911827219610436 \times 10^{-13}$

3. Result and discussion

The numerical solutions to the formulated problems discussed in the previous sections are examined. Figure 2 to Figure 5 illustrate the effect of the following values of the parameters $Sc = 5, Pr = 6.8, Tr = 2, m = 0.5, \lambda = 1, \alpha = 0.1, \delta_2 = -0.5, S = 0, Nt = 0.01, Nb = 0.01, Pp = 0.1, \delta_1 = 0.1, \beta = 0.5, M = 0.5, \sigma^* = 0.1$ and $E = 0.1$ are default values used in this study and the parameters remain fixed throughout the research unless otherwise stated. Table 2 and Table 3 display the non-Newtonian CF and Newtonian fluid $(\beta = \infty)$ for local Nusselt number and skin friction co-efficient, with various values of M, S, N, and E_c respectively. For both cases of non-Newtonian CF and Newtonian fluid $(\beta = \infty)$, it is found that the magnetic field parameter (M) rises with the value of the Nusselt-number $Nu_{\overline{x}}$ Whereas, the magnetic field parameter reduces the Skin friction coefficient in both cases. It was found that the magnetic field tends to oppose the damping force. From Table 2 and Table 3, the viscous dissipation in term of Eckert number enhances Skin friction coefficient C_f and reduce the magnitude of Nusselt-number $Nu_{\overline{x}}$. The values of the Skin friction coefficient C_f and Nusselt-number $Nu_{\overline{x}}$ increase gradually for rising values of suction/injection parameter for both cases. Also, we observed the suction/injection parameter moves smoothly towards the direction of the wall temperature [19] presented in Table 3 and Table 4. Besides, both the magnitude of Skin friction coefficient C_f and local Nusselt number Nu values increses with incresing thermal radiation parameter. As expected, the thermal radiation increases gradually with the high temperature in the channel walls [9]. Finally, the impact of Non-Newtonian CF on the Skin friction coefficient C_f and Nusselt-number $Nu_{\overline{x}}$ are very noticeable when compared to the Newtonian fluid. CF acquires high shearing within the fluid channel as the case with blood models [26]. likewise, Casson liquid fluid enhances the heat transfer rate to generate vasodilation [4]. 4 exhibit the comparison of current studies and previously published results. ([Uddin *et al.* [19]] and Bejan [26] for Pr when $K =$

$Nr = Ec = M = \alpha = 0, Nt = Nb \to 0, \lambda = a = b = c = 0, Da = N = \beta \to \infty$ an excellent agreement can be observed. Skin friction coefficient C_f and Nusselt number (Nu).

Table *2.* Computed numerical values of Skin friction coefficient C_f and Nusselt number $Nu_{\bar{x}}$ when $R, Ec, M, S, \epsilon = 0.1$, $Pr = 0.71$, $G = 1$ Casson liquid fluid=1.5

M	S	E_c	R	Skin-friction co-efficient C_f	Nusselt-number $Nu_{\bar{x}}$
4.0	0.6	0.3	0.2	0.481466	1.56967
5.0	0.6	0.3	0.2	0.531545	1.48331
6.0	0.6	0.3	0.2	0.559841	1.39887
4.0	**0.3**	0.3	0.2	0.278461	1.54178
4.0	**0.9**	0.3	0.2	0.669694	1.62189
4.0	**1.5**	0.3	0.2	0.765255	1.69619
4.0	0.6	**0.0**	0.2	0.490456	1.79518
4.0	0.6	**0.6**	0.2	0.490456	0.99749
4.0	0.6	**1.5**	0.2	0.490456	0.39923
4.0	0.6	0.3	**0.0**	0.811848	0.94631
4.0	0.6	0.3	**0.5**	0.236111	1.24429
4.0	0.6	0.3	**0.9**	0.173479	1.69884

Table 3. Numerical values of Skin friction coefficient C_f and Nusselt number Nu for different values of: $M, S, R, Ec, \epsilon = 0.1$, $Pr = 0.71$, $G = 1$ Newtonian Fluid=∞

M	S	E_c	N	Skin friction coefficient C_f	Nusselt number $Nu_{\bar{x}}$
4.0	0.6	0.3	0.2	0.355176	1.46888
5.0	0.6	0.3	0.2	0.389367	1.36241
6.0	0.6	0.3	0.2	0.416519	1.26479
4.0	**0.3**	0.3	0.2	0.219918	1.43813
4.0	**0.9**	0.3	0.2	0.459863	1.53328
4.0	**1.5**	0.3	0.2	0.496965	1.61746
4.0	0.6	**0.0**	0.2	0.355178	1.67722
4.0	0.6	**0.6**	0.2	0.355178	0.95688
4.0	0.6	**1.5**	0.2	0.355101	0.43331
4.0	0.6	0.3	**0.0**	0.447734	0.96908
4.0	0.6	0.3	**0.5**	0.231347	1.23333
4.0	0.6	0.3	**0.9**	0.183491	1.56629

Table 4. Validation of reduced wall heat transfer rate $(-\theta'(0))$ for different values of Pr when $K = Nr = Ec = M = \alpha = 0, Nt = Nb \to 0, \lambda = a = b = c = 0, Da = N = \beta \to \infty$

Pr	Present study	Uddin *et al.* [19]	Bejan, [26]
0.01	0.1824	0.180	0.162
07.2	0.38737	0.387	0.387
1	0.40103	0.401	0.401
2	0.42601	0.426	0.426
10	0.46498	0.464	0.465
100	0.48932	0.489	0.490
1000	0.49521	0.497	0.499

Figure 1b. Display the graph of the residual functions $R(\eta)$. It was found that the residuals are minimized in the domain (0 to ∞). *Figure* $2(a, b, c, d)$ displayed the impacts of porosity first and second-order velocity slip parameters $(Pp, \delta_1$ and $\delta_2)$ on Casson flow velocity, temperature profile. Higher values of porosity parameter (Pp) lessening the Casson flow velocity (see *Fig.* $2a$) and elevating temperature profiles. These outcomes are perhaps as a result of to porosity parameter (Pp) being inversely proportional to fluid permeability (k_p). mounting po-rosity parameter, the porosity parameter enhances the resistance of Casson nanofluid to flow and leads to retardation. The fluid temperature increases since the flow is slightly stagnated and allow more heat to conducted to the fluid. Also, enhancement in the first-order slip

parameter elevates the fluid temperature (see Figure 2b.) These phenomena are for the reason that not all the dragging force from the stretching sheet can be spread to the Casson nanofluid [28].
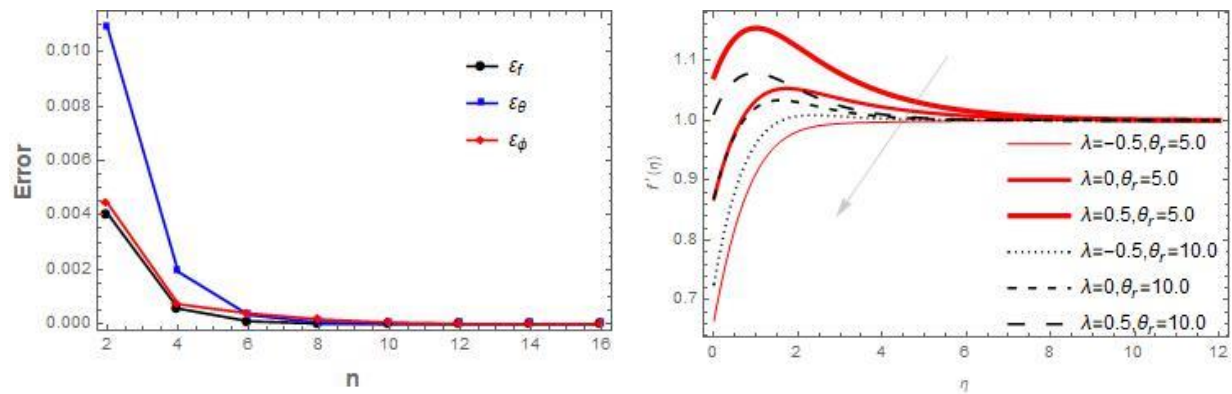

Figure 1(b, c). Minimized residual error $R(\eta)$ and impact of viscosity parameter on $(f'(\eta))$
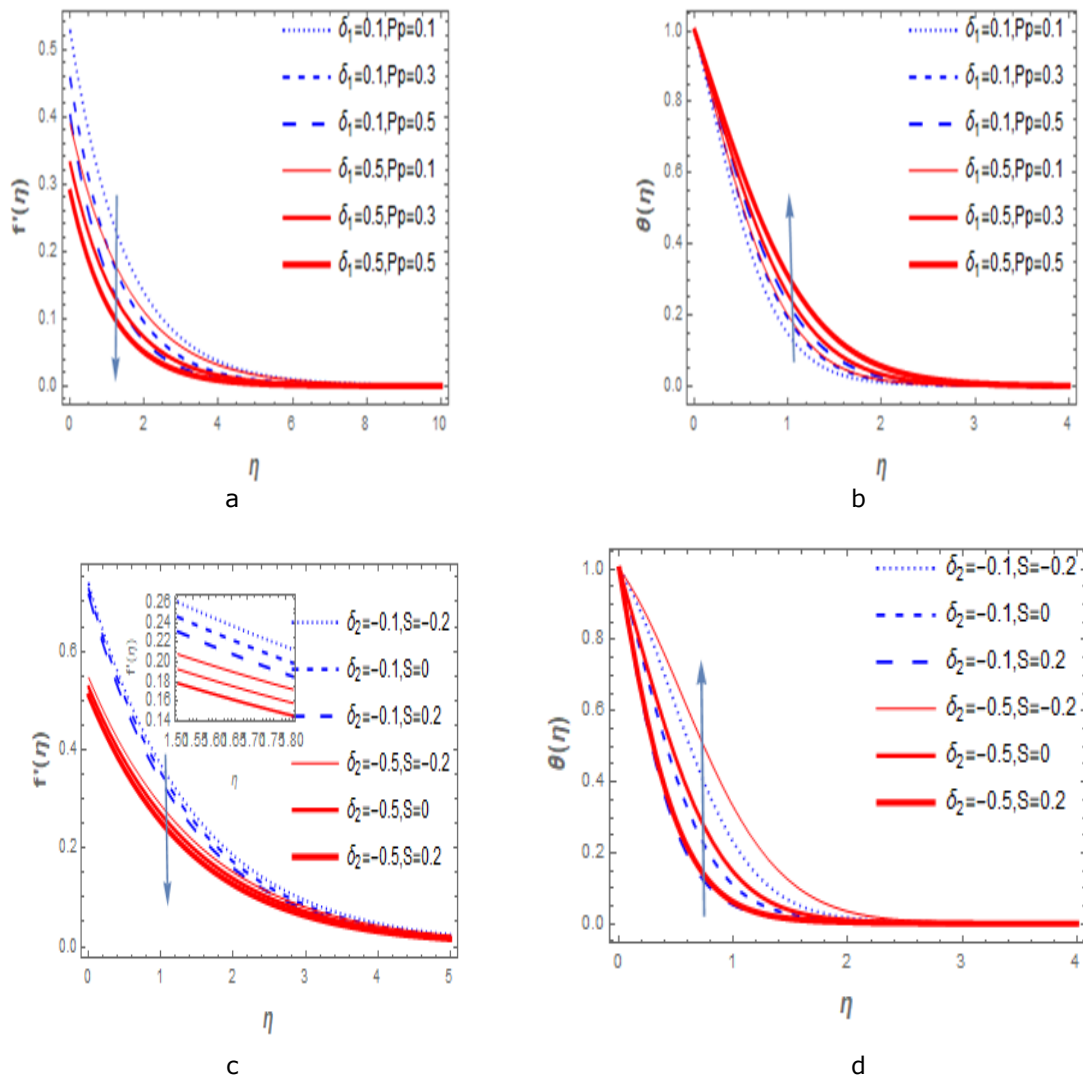

a

b

c

d

Figure 2. Impact of (a, b, c, and d) porosity, first, and second-order velocity slip parameters on fluid flow, temperature profile.

Figure 2(c,d) demonstrate the effect of second-order slip and wall transpiration (suction/injection) parameters (δ_2 and S) on fluid velocity, temperature profile, It is observed that the fluid flow is reduced and the temperature profile. As the second-order slip parameter increases for both wall injection ($S < 0$) and suction ($S > 0$). Also, the fluid velocity profile increases with injection while it decreases with suction. The opposite is the case for both temperature and nanoparticle volume fraction profiles. Comparable outcomes are found by [21].
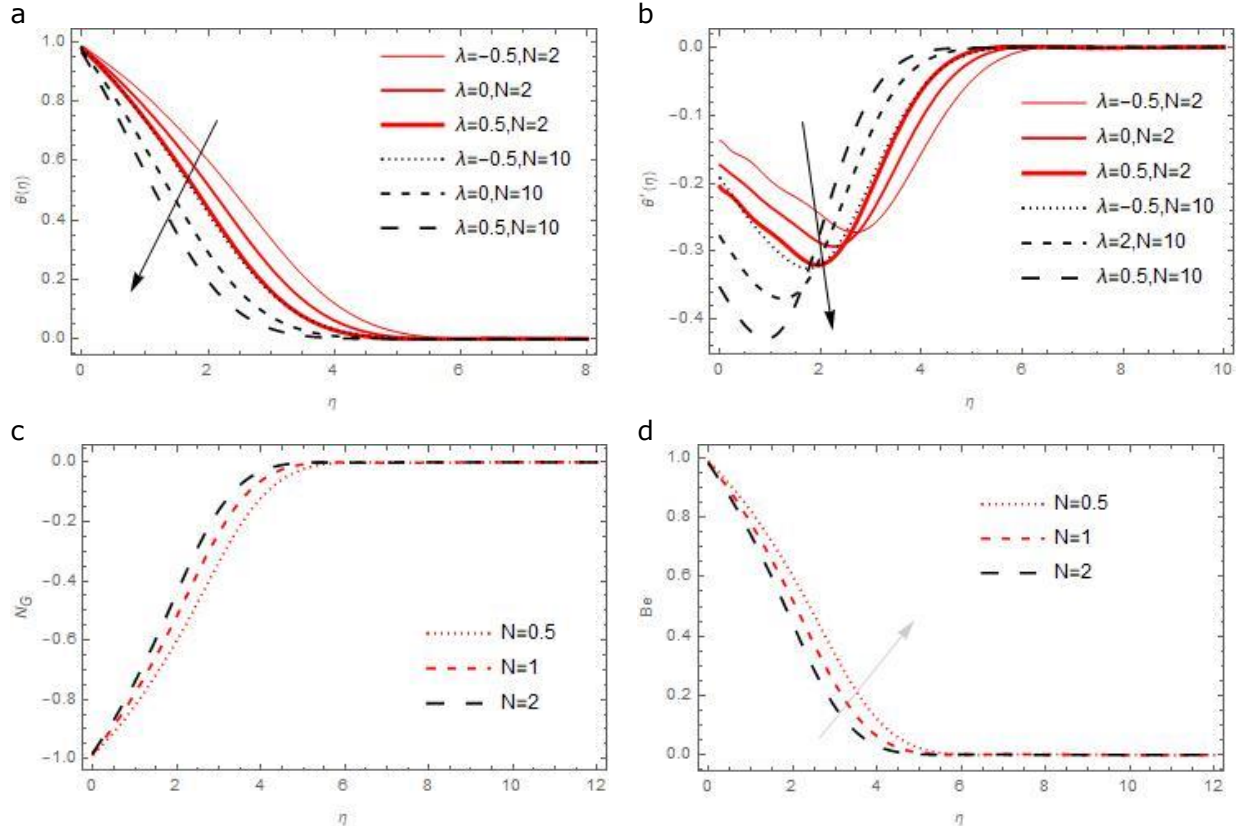

Figure 3(a, b, c, d). Effect of solar radiation parameter on ($\theta'(\eta)$), ($\theta(\eta)$), (N_G), and (Be)

It was found that an increase in solar radiation parameter enhances the absorbing rate (k) which decreases the fluid velocity ad temperature profile. Consequently, the thermal radiation parameter describes exactly the related additional conduction to thermal radiation [15] as displayed in Figure 3b. Figure 3c shown the effect of thermal radiation parameter on the entropy generation. The entropy production rate reduces at the boundary layer thickness with an increasing solar radiation parameter. The thermal radiation parameter accelerates the entropy generation, which causes an enhancement in the entropy production. Figure 3d demonstrated the effect of the radiative parameter on Bejan number profile. At the wall, the solar radiation parameter reduces the Bejan number profile. The existence of thermodynamics irreversibility dominates the heat transfer entropy production.

Figure 4(a, b). exhibit that the fluid flow slows down as the Casson and Magnetic field parameters (β and M) increases. This can be ascribed to the existence of Lorentz force which serves as a resisting force to the fluid flow. Hence, it slows down the fluid velocity, meanwhile its propensity to suppresses and decelerate the CF motion [25]. The impact of increasing magnetic field parameters is noticeably accelerated by the fluid temperature within the boundary layer. Because the existence of ohmic heating acts as an additional source of heat to the fluid temperature. The figure shows the impact of the CF parameter on the velocity profile. It is found that an increase in CF parameter contributes to an improvement in the fluid flow. Logically, the Casson rheological was used as a fluid by plastic dynamic viscosity which has a powerful reaction on yield stress [16]. However, as Casson rheological near infinity, the fluid

flow increases extremely. Figure 4(c, d). presents the impact of the magnetic field parameter on the entropy generation. The influence of the magnetic field parameter on entropy generation weaker the wall at the boundary layer, furthermore the magnetic field parameter strongly reduces the system stability at the molecular level. For the case of Bejan number, it was found that the magnetic field parameter elevates the Bejan number profile. Also, the Bejan number strongly increased at the boundary layer thickness.
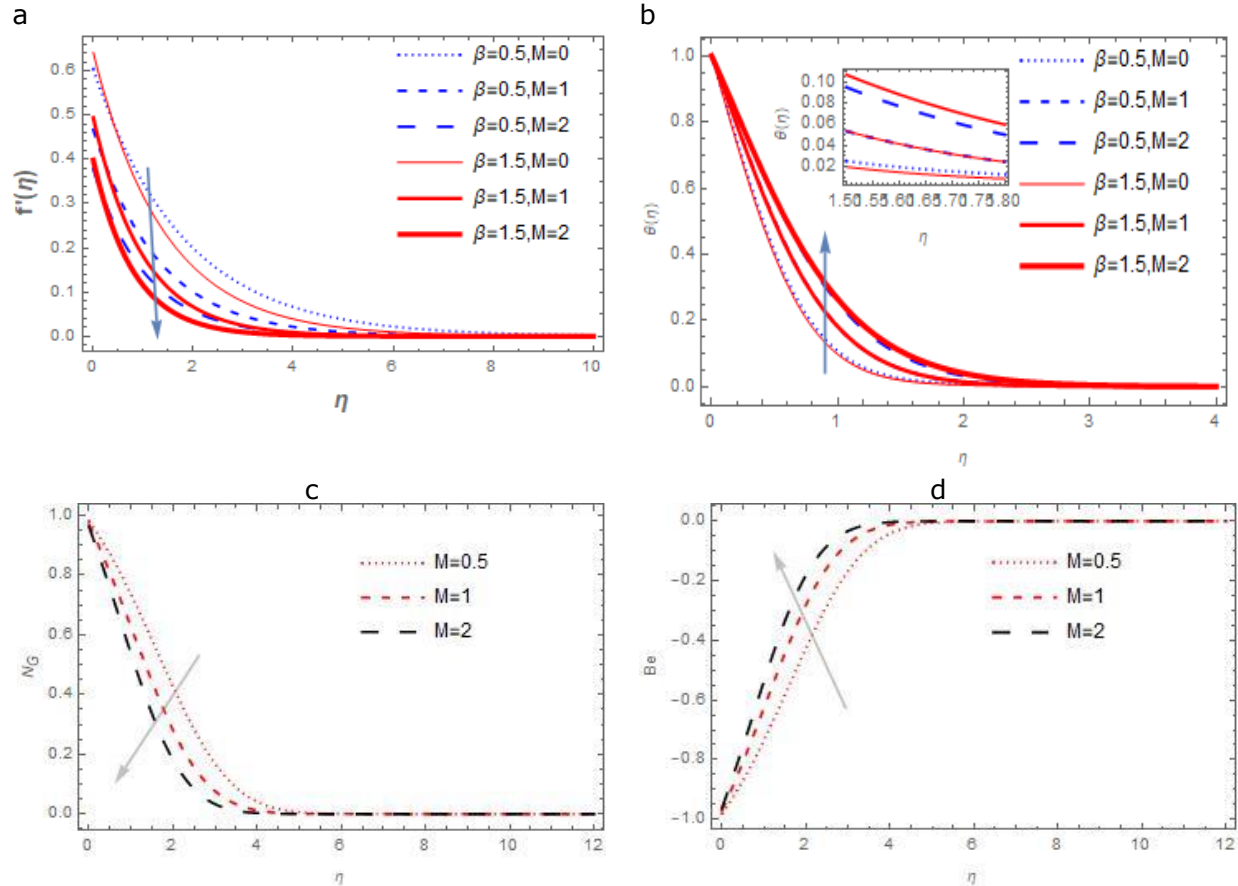

Figure 4(a, b, c, d). Effect of Casson parameter and Magnetic parameter on $(\theta'(\eta))$, $(\theta(\eta))$, (N_G), and (Be)
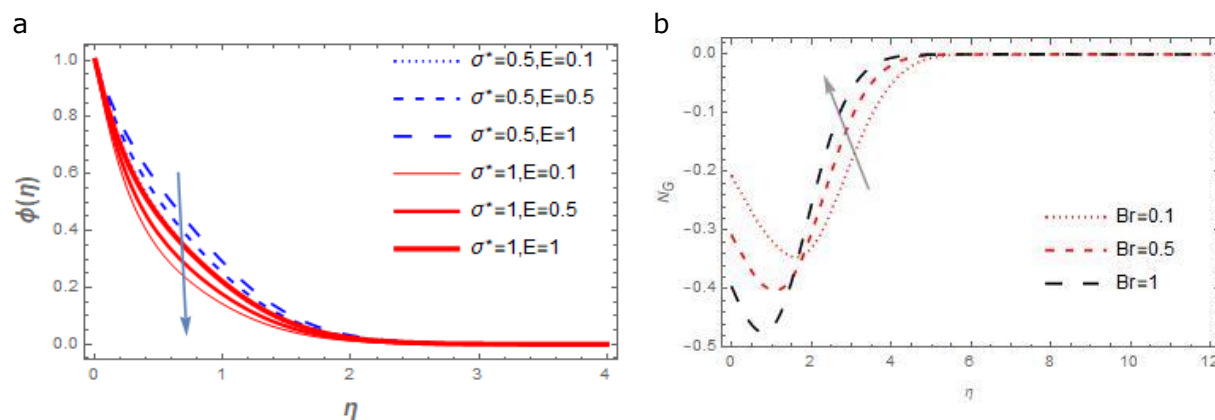

Figure 5(a, b). Effect of chemical reaction and activation energy parameters $(\sigma^* \text{and} E)$ On $\phi(\eta)$

The influence of chemical reaction and activation energy parameters $(\sigma^* \text{and} E)$ on the nanoparticle volume fraction profile presented in Figure 5(a, b). It is found from the last term of

Eq. (16) that the term $Sc\sigma^{*2}\left((Tr-1)\theta+1\right)^{m}e^{\frac{-E}{(Tr-1)\theta+1}}$ is increased as σ^{*} elevated. This leads to a decrease in the nanoparticle volume fraction profile. Furthermore, nanoparticle volume fraction profile is increased with increasing activation energy parameter (E) as it is observed in Fig. 16. Activation energy is known as the energy that must be overcome before a chemical reaction can occur. To have a reasonable chemical reaction, there must be an appreciable number of molecules with energy equal to or greater than the activation energy. An increase in activation energy parameter (E) results to a decrease in $Sc\sigma^{*2}\left((Tr-1)\theta+1\right)^{m}e^{\frac{-E}{(Tr-1)\theta+1}}$ which later leads to an increase in the nanoparticle volume fraction profile.
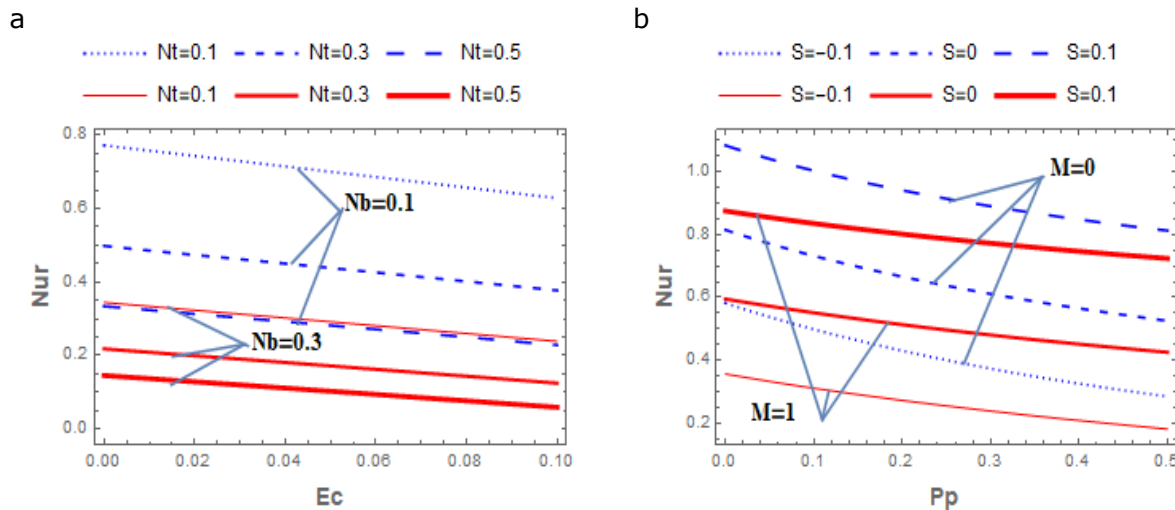

Figure 6. Impact of (a and b) Pp, S and M On Nusselt number profile.

Figures 6(a, b) present the effects of these various parameters $(Nt, Nb, Ec, Pp, M \text{ and } S)$ on the Nusselt number. It is observed that Nusselt number is a decreasing function of Brownian motion, thermophoresis, Eckert number, Magnetic field, porosity, and injection parameters $(Nb, Nt, Ec, M, Pp, S < 0)$ while it is an increasing function of the only suction parameter $(S > 0)$. Also, Figs 21 and 22 depict the effects of parameters $\sigma^{*}, E, Nt, Kr, Pp, M \text{ and } S$ on Sherwood number. It is noticed that Sherwood number is increased as each of chemical reaction rate parameter (σ^{*}), thermophoresis parameter (Nt) and suction parameter (S>0) increases, while it is decreased with increasing activation energy parameter (E), porosity parameter (Pp), Magnetic field parameter (M), and injection parameter (S<0).

4. Conclusion

In this work, we have successfully employed a Casson rheological model to analyze the second law thermodynamics for a steady, incompressible flow, electrically conducting viscosity fluid. Using GWRM numerical solution for dimensionless conservation equations have been obtained and observed against various thermophysical parameters. The significant results are itemized below:

1. The research has exhibits that the CF velocity reduces with increasing values of first-order velocity slip parameter (δ_1), second $-$ order velocity slip parameter (δ_2), Casson parameter (β), Magnetic field Parameter (M), while it increases with increasing values of wall injection parameter, β, and Bi_0.

2. The fluid temperature increases with higher values of porosity parameter (Pp), velocity slip parameter, (δ_1), second $-$ order velocity slip parameter (δ_2), Casson-parameter (β), Magnetic field, suction parameter but reduced for injection case

3. Increasing chemical reaction parameter (σ^{*}), thermophoresis parameter (Nt) and suction parameter (S>0) increase Sherwood number profile while increasing activation energy

parameter (E), porosity parameter (Pp), Magnetic field parameter (M), and injection parameter (S<0) reduce Sherwood number.
4. The system stability at the molecular level reduces for Magnetic field parameter (M), however, significant amplification is described for Brinkman number, solar radiation parameter (N)
5. the profile of the bejan number is control by higher values of the Brinkman number, solar radiation parameter (N), and Magnetic field parameter (M).
6. The result of the Magnetic field Parameter (M), suction parameter $(S > 0)$, Solar radiation parameter Skin friction coefficient (c_f) and local Nusselt number (Nu) more pronounced for Casson fluid when compared to a Newtonian fluid
7. The obtained results show a significant influence in describing the strong interest of the occurrence of solar radiation and it conveys into the work of nanofluid by convection.

Nomenclature

$\bar{u}$ and $\bar{v}$ are the velocity component in $\bar{x}$ and $\bar{y}$ direction
τ ratio of nanoparticle heat capacity
ρ_f density
B_0 constant magnetic field
g gravity
D_B Brownian diffusion
U_r reference velocity
Pr Prandtl number
Nb Brownian motion
E activation energy
σ^* chemical reaction
δ_1 frist-order velocity slip
δ_2 second-order velocity slip

α thermal diffusivity thermal diffusivity
ν kinematic viscosity
σ_0 electric conductivity
$(k_p)_o$ permeability of the porous medium
D_T thermophoresis diffusion
λ stretching sheet parameter
Kr chemical reaction
$\bar{u}_{slip}$ velocity slip at the wall
Re Reynolds number
Nt thermophoresis parameter
M magnetic parameter
Pp porosity parameter
Ec Eckert number

Acknowledgment

Conflict of interest: The authors declare none

References

[1]   Bejan A. Second-law analysis in heat transfer and thermal design. Advances in heat transfer, 2015; 15(1): 1-58.
[2]   Abolbashari MH, Freidoonimehr N, Nazari F, and Rashidi MT. Analytical modeling of entropy generation for Casson nano-fluid flow induced by a stretching surface. Advanced Powder Technology, 2015; 26(2): 542-552.
[3]   Aziz A, Makinde OD. Heat transfer, Analysis of entropy generation and thermal stability in a slab. Journal of thermophysics heat transfer, 2010; 24(2): 438-444.
[4]   Abd El-Aziz M and Afify AA. MHD Casson fluid flow over a stretching sheet with entropy generation analysis and Hall influence. Entropy, 2019;21(6): 592.
[5]   Adesanya SO, Falade J, Jangili S, and Beg OA. Irreversibility analysis for reactive third-grade fluid flow and heat transfer with convective wall cooling, Alexandria Engineering Journal, 2017; 56(1): 153-160.
[6]   Bhattacharyya K. MHD stagnation-point flow of a Casson fluid and heat transfer over a stretching sheet with thermal radiation. Journal of Thermodynamic, 2013: 169674.
[7]   Saleem M, Hossain M, Saha SC, Gu Y. Heat transfer analysis of viscous incompressible fluid by combined natural convection and radiation in an open cavity. Mathematical Problems in Engineering, 2014; 412480.
[8]   Turkyilmazoglu M. Thermal radiation effects on the time-dependent MHD permeable flow having variable viscosity. International Journal of Thermal Sciences, 2011; 50: 88-96.
[9]   Khan M, Malik MY, and Salahuddi, T. Heat generation and solar radiation effects on Carreau nanofluid over a stretching sheet with variable thickness: using coefficients improved by Cash and Carp. Results in physics, 2017; 7:.2512-2519.

[10]   Akhter R, Mohammad MA, Babul H, and Musa M. MHD free convection boundary layer flow over an inclined heated flat plate with thermal radiation. Americal Journal of fluid Dynamics, 2017; 44: 583-595.

[11]   Mondal S, Haroun N. A, Sibanda P. The effects of thermal radiation on an unsteady MHD axisymmetric stagnation-point flow over a shrinking sheet in presence of temperature dependent thermal conductivity with Navier slip. PLoS, 2015; 9: 553-685.

[12]   Malik MY, Naseer M, Nadeem S, Rehman A. The Boundary Layer Flow of Casson Nanofluid over a Vertical Exponentially Stretching Cylinder. Appl. Nanosci., 2014; 4: 869–873.

[13]   Oyelakin IS, Mondal S., and Sibanda P. Unsteady Casson nanofluid flow over a stretching sheet with thermal radiation, convective and slip boundary conditions. Alexandria Engineering Journal, 2016; 55(2): 1025-1035.

[14]   Casson N. A flow equation for pigment-oil suspensions of the printing ink type. In: Mill, C.C., Ed., Rheology of Disperse Systems, Pergamon Press, Oxford, 84-104.

[15]   Animasaun IL. Effect of thermophoresis, variable viscosity and thermal conductivity on free convective heat and mass transfer of non-Darcian MHD dissipative Casson fluid flow with suction and nth order chemical reaction. Journal of Nigeria Mathematical Society, 2015; 34: 11-31.

[16]   Ibukun SO, Sabiyasachi M, and Precious S. Unsteady Casson nanofluid flow over a stretching sheet with thermal radiation, convective and slip boundary conditions, Alexandria Engineering Journal, 2016; 55: 1025-1035.

[17]   Raju RS. Unsteady MHD boundary layer flow of Casson fluid over an inclined surface embedded in a porous medium with thermal radiation and chemical reaction. Journal of Nanofluids, 2018; 7(4): 694-703.

[18]   Mukhopadhyay S, Vajravelu K, van Gorder AM. Casson fluid flow and heat transfer at an exponentially stretching permeable surface. Journal of Applied Mechanics and Technical Physics, 2013; 80: 344-786.

[19]   Abolbashari MH, Freidoonimehr N, Nazari F, and Rashidi MT. Analytical modeling of entropy generation for Casson nano-fluid flow induced by a stretching surface, Advanced Powder Technology, 2015; 26(2): 542-552.

[20]   Shaw S, Mahanta G, Sibanda PJ. Non-linear thermal convection in a Casson fluid flow over a horizontal plate with convective boundary condition. Alexandria Engineering Journal, 2016; 55(2): 1295-1304.

[21]   Obalalu AM, Ajala OA, Adeosun AT, Wahaab FA, Aliu O, and Adebayo LL. Natural Convective Non-Newtonian Casson Fluid Flow in a Porous Medium with Slip and Temperature Jump Boundary Conditions. Pet Coal, 2020; 62(4): 1532-1545.

[22]   Gireesha B, Kumar KG, Krishnamurthy M, Manjunatha S, and Rudraswamy N. Impact of ohmic heating on MHD mixed convection flow of Casson fluid by considering Cross diffusion effect. J Nonlinear Engineering, 2019; 8(1): 380-388.

[23]   Pop I, Sheremet N. Free convection in a square cavity filled with a Casson fluid under the effects of thermal radiation and viscous dissipation. International Journal of Numerical Methods for Heat Fluid Flow, 2017; 25: 25-34.

[24]   Shrama P, and Singh G. Steady MHD natural convection flow with variable electrical conductivity and heat generation along an isothermal vertical plate. J Journal of Applied Science Engineering, 2010; 13 (3): 235-242.

[25]   Obalalu AM, Wahaab FA, Adebayo LL. Heat transfer in an unsteady vertical porous channelwith injection/suction in the presence of heat generation. Journal of Taibah University for Science, 2020; 14: 541-548.

[26]   Uddin MJ, Beg OA, and Ismail AI. Radiative convective nanofluid flow past a stretching/shrinking sheet with slip effect. J. Thermophysics and Heat Transfer, 2015; 29(3): 513-523.

[27]   Jung AC, Ribeiro C, Michaut L, Certa U, Affolter M. Polycheatoid/z0-1 is requied for cell specification and rearrangement during Drosphila tracheal morphogenesis. Curr .Biol., 2006; 16(12): 1224-1231.

[28]   Yurong H, Yi J, Chen Y, Yulog D, Daqiang C, Lu H. Heat transfer and flow behaviour of aqueous suspensions of TiO_2 nanoparticles (nanofluids) flowing upward through a vertical pipe. International Journal of Heat And Mass Transfer, 2007; 50 (11-12): 2272-2281.

[29]   Wahaab FA, Adebayo LL, Adekoya AA, Hakeem IG, Alqasem B, and Obalalu AM. Physiochemical properties and electromagnetic wave absorption performance of Ni0. 5Cu0. $5Fe_2O_4$ nanoparticles at X-band frequency. Journal of Alloys and Compounds, 2020; 155272.

[30]   Zan G, Wu T, Hu P, Zhou Y, Zhao S, Xu S, Chen J, Cui Y, and Wu Q. An approaching-theoret-ical-capacity anode material for aqueous battery: Hollow hexagonal prism Bi_2O_3 assembled by nanoparticles. Energy Storage Materials, 2020; 28: 82-90.

[31]   Wahaab FA, Adebayo LL, Adekoya AA, Yusuf JY, Obalalu AM, Yusuff AO, and Alqasem B. Electromagnetic wave-induced nanofluid-oil interfacial tension reduction for enhanced oil re-covery. Journal of Molecular Liquids, 2020; 318: 114378.

[32]   Kataria HR, and Patel EJ. Radiation and chemical reaction effects on MHD Casson fluid flow past an oscillating vertical plate embedded in porous medium. Alexandria Engineering Jour-nal, 2016; 55(1): 583-595.

[33]   Bestman A. Natural convection boundary layer with suction and mass transfer in a porous medium," International journal of energy research, 1990; 14(4): 389-396.

[34]   Berger BS. The inversion of the Laplace Transform with applications to the vibrations of con-tinuous elastic bodies. J. Appl. Mech., 1968; 35(4): 837-839.

[35]   Segerlind LJ. Weighted residual solutions in the time domain. International journal for nu-merical methods in engineering, 1989; 28(3): 679-685.

[36]   Brooks AN, and Hughes TJ. Streamline upwind/Petrov-Galerkin formulations for convection dominated flows with particular emphasis on the incompressible Navier-Stokes equa-tions. Computer methods in applied mechanics and engineering, 1982; 32(1-3): 199-259.

[37]   Mino Y, and Shinto H. Lattice Boltzmann method for simulation of wettable particles at a fluid-fluid interface under gravity. Physical Review E, 2020; 101(3): 033304.

[38]   Pruess S, and Fulton CT. Mathematical software for Sturm-Liouville problems. ACM Transac-tions on Mathematical Software (TOMS), 1993; 19(3): 360-376.

[39]   Aladjev V. June. Computer Algebra System Maple: A New Software Library. In International Conference on Computational Science 2003(pp. 711-717). Springer, Berlin, Heidelberg.

[40]   Obalalu AM, Kazeem I, Abdulrazaq A, Ajala OA, Oluwaseyi A, Adeosun AT, Adebayo LL, and FA. Numerical simulation of entropy generation for Casson fluid flow through permeable walls and convective heating with thermal radiation effect. Journal of the Serbian Society for Com-putational Mechanics, 2020; 14 (2): 503-519.

[41]   Salufu SO, Isehunwa SO and Braimah J. Effect of water and gas-oil and Gas Recovery factors optimation. Petroleum and Coal, 2020; 62(1:) 233-237

[42]   Ajala OA, Obalalu AM, Abimbade SF, and Akinyemi OT. Numerical Study of Forced Convective Heat Generation Flow through a Permeable Walls with Suction/Injection, International Journal of Scientific and Research Publications, 2019; 9: 336-348.

[43]   Ajala O, Adegbite P, Abimbade S, and Obalalu A. Thermal Radiation and Convective Heating on Hydro magnetic Boundary Layer Flow of Nanofluid past a Permeable Stretching Surface. Int. Journal of Applied Mathematics & Statistical Sciences, 2019; 101(3):033304.

[44]   Ajala O, Abimbade S, Obalalu A, and Adeosun A. Existence and uniqueness of forced convec-tive flow through a channel with permeable walls in presence of heat generation. Int. Journal of Engineering Applied Sciences and Technology, 2019; 361-374.

[45]   Olar HR, Halafawi M, Avram L. Investigating Dynamic Analysis of Well Performance Producing from Turdaş Structure in Turdaş Gas Field Using a Production Logging Tool. Pet Coal; 2021; 63(1): 278-283.

[46]   Zhang W-M, Meng G, Wei X. A review on slip models for gas microflows, Microfluidics Nanofluidics; 2012; 13(6): 845-882.

To whom correspondence should be addressed: Dr. Adebowale Martins Obalalu, Department of Statistics and Math-ematical Sciences, Kwara State University, Malete, Nigeria, E-mail: adebowale.obalalu17@kwasu.edu.ng